


RESEARCH LETTER

Open Access



Seasonal mixed layer temperature and salt balances in the Banda Sea observed by an Argo float

Mochamad Furqon Azis Ismail^{1,2*} , Johannes Karstensen¹, Joachim Ribbe³, Taslim Arifin², Handy Chandra², Rudhy Akhwady², Erma Yulihastin², Abdul Basit² and Asep Sandra Budiman²

Abstract

For the first time, the processes controlling the variations of mixed layer temperature (MLT) and salinity (MLS) in the Banda Sea are quantified using data from a single Argo float in combination with satellite and reanalysis outputs from August 2017 to August 2019. This augments previous studies that utilized ocean model data only. We document the presence of a barrier layer and quantify the roles of air-sea heat and mass exchanges, horizontal advection, and vertical entrainment in the seasonal variability of MLT and MLS. We find that heat gains and losses at the air-sea interface are the main contributor to the warming and cooling of the MLT. Seasonal changes in MLS are driven by advection of low salinity water rather than freshwater fluxes from precipitation and evaporation. This is particularly the case during the late northwest and monsoon transition period from February to April when low salinity is advected eastward from the Java Sea into the Banda Sea.

Keywords Mixed layer temperature, Barrier layer, Argo float, The Banda Sea, Monsoon

Introduction

The Banda Sea is a large and deep marginal basin in the region of the Indonesian Maritime Continent (IMC). It is confined to the north of the Timor Passage by an arc of islands that separate the Banda Sea from the Arafura Sea in the east, the Maluku Sea in the north and the Flores Sea in the west (Fig. 1a). This region is unique due to its complex topography, land-marine biodiversity, distinct upper ocean circulation, and atmospheric processes over the IMC that potentially influence climate processes on a global scale (Lee et al. 2019; Yoneyama and Zhang

2020). Ocean circulation in the Banda Sea is part of the branch of the Indonesian Throughflow (ITF), an intrinsic part of the global ocean circulation that transports heat from the Pacific Ocean into the south-eastern tropical Indian Ocean (Yuan et al. 2018, 2022). The ITF exerts its influence primarily on the interior circulation of the western and southern boundaries of the Banda Sea (Zhu et al. 2019).

There is an interest in distinguishing the role of the ITF heat transport anomalies that originate in the Pacific Ocean from those that are due to global atmospheric warming and local air-to-sea heat fluxes. The seasonal monsoonal wind is the primary cause of the surface circulation pattern along the eastern boundary of the Banda Sea (Zhu et al. 2019). From December to March, the northwest monsoon driven Ekman flow results in warm water to accumulate in the Banda Sea, which reduces the overall ITF transport (Sprintall and Liu 2005). In contrast, the export of water from the Banda Sea toward the Indian Ocean is strongest during the

*Correspondence:

Mochamad Furqon Azis Ismail
fismail@geomar.de

¹ GEOMAR Helmholtz Centre for Ocean Research Kiel, 24148 Kiel, Germany

² National Research and Innovation Agency of Indonesia, Jakarta 10340, Indonesia

³ School of Sciences, University of Southern Queensland, Toowoomba, QLD 4350, Australia



© The Author(s) 2023. **Open Access** This article is licensed under a Creative Commons Attribution 4.0 International License, which permits use, sharing, adaptation, distribution and reproduction in any medium or format, as long as you give appropriate credit to the original author(s) and the source, provide a link to the Creative Commons licence, and indicate if changes were made. The images or other third party material in this article are included in the article's Creative Commons licence, unless indicated otherwise in a credit line to the material. If material is not included in the article's Creative Commons licence and your intended use is not permitted by statutory regulation or exceeds the permitted use, you will need to obtain permission directly from the copyright holder. To view a copy of this licence, visit <http://creativecommons.org/licenses/by/4.0/>.

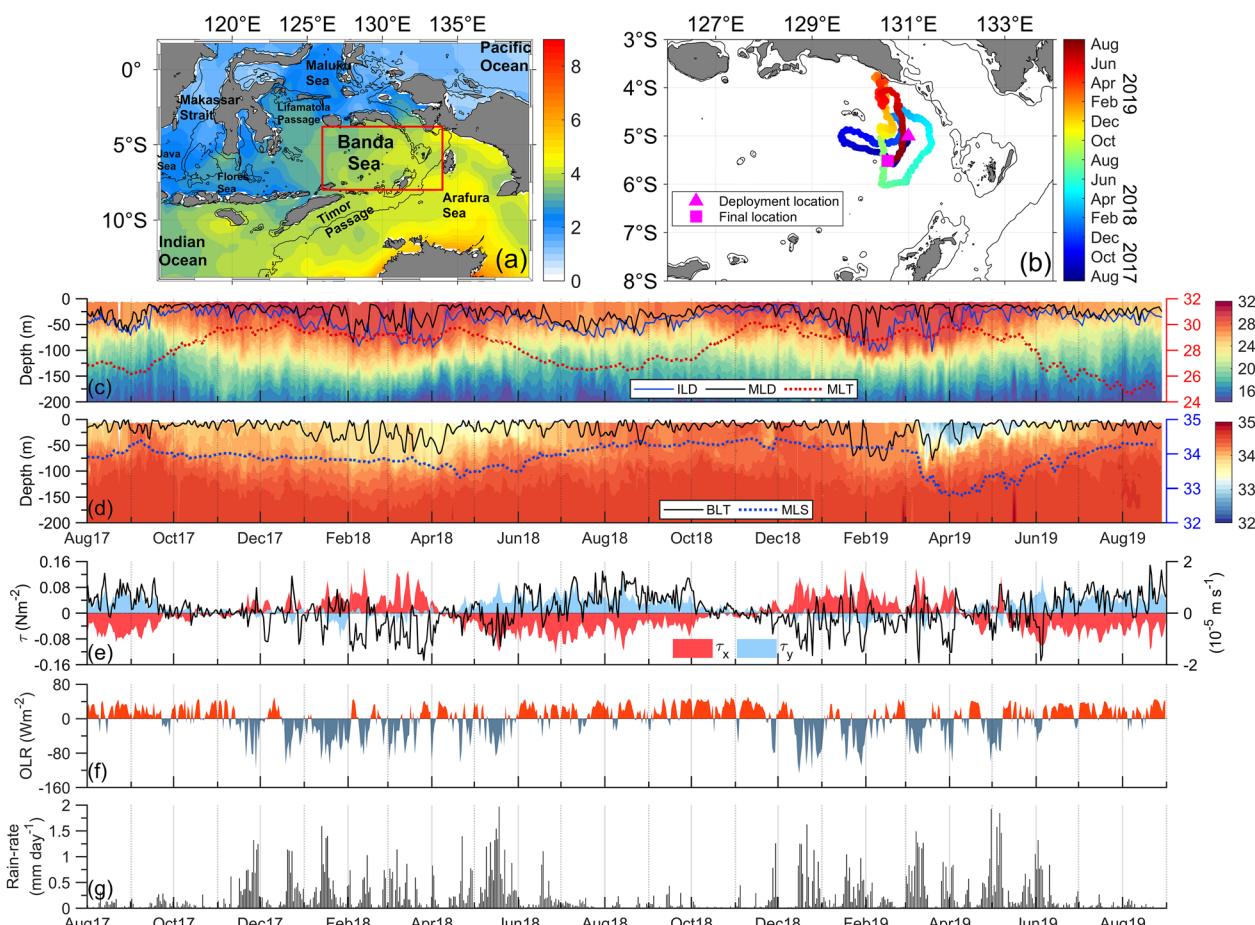


Fig. 1 **a** Map of the Indonesian Maritime Continent showing the amplitude of the seasonal cycle of SST (°C). **b** The trajectory of the Argo float (WMO ID 6901746) from August 2017 to August 2019. Solid black contours in **a**, **b** show the 500 m isobath. Time-depth sections of **c** daily temperature (°C) and **d** daily salinity (psu) along the trajectory of the Argo float 6901746. **e** Temporal evolution of daily zonal and meridional wind stress ($N m^{-2}$). **f** Daily OLR anomaly ($W m^{-2}$), and **g** daily precipitation ($mm day^{-1}$). The area boxed by red lines indicates the location of the area captured in **b**. The blue and black lines in **c** denote the ILD and MLD, respectively. The black line in **d** denotes the BLT. The dotted red and blue lines in **c** and **d** indicate the MLT (°C) and MLS (psu), respectively. The black line in **e** denotes the vertical velocities ($m s^{-1}$) associated with Ekman pumping. All plots in Figs. 2 and 3 are based on a monthly average from the original daily data

southeast monsoon from about June to September (Sprintall and Liu 2005). Apart from the ITF, the barrier layer thickness (BLT) and isothermal layer depth (ILD) are notable factors influencing the sea surface temperature (SST) in the IMC (Qu et al. 2005). Sprintall and Tomczak (1992) argued that monsoon-related rainfall and river runoff likely contribute to its existence in the region.

The Banda Sea is characterized by a seasonal cycle in SST (Fig. 1a), which is not as evident in the surrounding tropical regions of the eastern Indian Ocean and western Pacific Ocean (Qu et al. 2005; Halkides et al. 2011). Previous studies found that the seasonal SST cycle is linked to the seasonally reversing monsoonal winds (Gordon and Susanto 2001; Kida and Richards 2009).

These are associated with the Madden–Julian Oscillation (MJO; Napitu et al. 2015) and the El Niño Southern Oscillation (ENSO, Gordon and Susanto 2001). SST evolution is controlled by an interplay of oceanic and atmospheric processes at the sea surface and processes within the mixed layer (Vijith et al. 2020; Oliver et al. 2021). In addition, the atmospheric structure and its circulation are sensitive to the mixed layer temperature (MLT) and ultimately the upper ocean heat balance as suggested by model experiments (Jochum and Potemra 2008).

The Banda Sea MLT influences air-to-sea heat and moisture fluxes. Both may drive deep atmospheric convection above the IMC (Kawamura et al. 2002) and thus potentially link with weather and climate

processes, even at the global scale (Yoneyama and Zhang 2020). The MLT impacts the redistribution of heat and freshwater that enter the eastern tropical Indian Ocean and originate in the western Pacific Ocean (Jochum and Potemra 2008). The Banda Sea MLT appears to be also related with drought and fire activity in Equatorial Asia (Kim et al. 2019). The MLT in the Banda Sea has been investigated with an emphasis on its temporal variability. Napitu et al. (2015) observed significant intraseasonal MLT variations in the Banda Sea during austral summer in response to the anomalous surface heat flux due to the MJO. Further, Pei et al. (2021) argued that substantial intraseasonal SST cooling occurred mainly due to the enhanced entrainment of colder waters associated with the MJO.

Previous studies of MLT changes and the temperature balance in the Banda Sea utilized ocean model data only (e.g., Halkides et al. 2011; Napitu et al. 2015). However, in making use of the global array of Argo floats, we identified one float (WMO ID 6901746) in the Banda Sea. To our knowledge, it provides the only coherent long-term record of in situ observations in the Banda Sea and covers the period August 1, 2017 to August 28, 2019 (Fig. 1b). The float data provide a highly resolved time series of in situ hydrographic data and allows to estimate mixed layer depth (MLD), ILD and BLT. Combining the float data analysis with atmospheric and ocean reanalysis data enabled studying the upper ocean processes that drive Banda Sea MLT and mixed layer salinity (MLS). Our focus here is on the relative importance of the heat and salt balance terms and how they differ on seasonal time scales.

Data and methods

This study uses pressure, temperature, and salinity profiles measured by a single Argo float 6901746 in combination with ocean and atmospheric reanalysis products and satellite data, see supporting information (Additional file 1: Text S1). In brief, following Shee et al. (2019), the data are averaged over a spatial grid of 0.5° for each position of the Argo float to obtain the air-sea heat exchange, horizontal advection, and vertical entrainment along the Argo float trajectory. The temperature balance is estimated as follows (Moisan and Niiler 1998):

$$\underbrace{\frac{\partial T_{\text{mld}}}{\partial t}}_a = \underbrace{\frac{Q_{\text{Net}}}{\rho_0 c_p h}}_b - \underbrace{\left(u_{\text{mld}} \frac{\partial T_{\text{mld}}}{\partial x} + v_{\text{mld}} \frac{\partial T_{\text{mld}}}{\partial y} \right)}_c - \underbrace{\left(\frac{T_{\text{mld}} - T_{-h}}{h} \left(w_{-h} + \frac{\partial h}{\partial t} \right) \right)}_d + \underbrace{\text{RES}}_e \quad (1)$$

The individual terms in Eq. 1 (from left to right) are (a) MLT tendency or the rate of change of the MLT, (b) net surface heat flux (NSHF), (c) total horizontal temperature advection (HTA) due to zonal temperature (ZTA) and meridional temperature (MTA) advections, (d) vertical temperature entrainment (VTE), and (e) unresolved residual. The salt balance equation is identical to Eq. 1, except temperature is replaced by salinity and the NSHF term is substituted by the net freshwater flux (FWF) denoting the net effects of precipitation, evaporation, and freshwater run-off (see Additional file 1: Text S2).

Results

Lagrangian trajectory and upper layer evolution from Argo float

During the period August 1, 2017 to August 28, 2019, the Argo float traverses the Banda Sea from its initial position at 5.00°S , 130.99°E to its final one at 5.51°S , 130.57°E (Fig. 1b). The positions of the float were limited to a $2^\circ \times 2^\circ$ domain and confined to the eastern Banda Sea. It covered a total distance of about 1,261 km and operated in an area of about 311 km^2 . The trajectory of the float indicates the presence of both cyclonic and anticyclonic eddy-like circulation features within the surface layer of the Banda Sea (Fig. 1b). The average speed of the float was approximately 0.02 m s^{-1} along numerous clockwise and anti-clockwise semi-circular flows (Fig. 1b). Time-depth distributions of temperature and salinity in the upper 200 m are shown in Fig. 1c and d. The time series of MLT, MLS, MLD, ILD, and BLT are overlaid in both figures. The temporal changes exhibit semi-annual variations that appear to be limited to the top 100 m. The warming of MLT and the shallowing of MLD exhibit a bimodal distribution. The mean MLD is 26.14 m throughout the Argo observation period.

Following Sprintall and Liu (2005), four distinct periods can be identified that align with particular states of the atmospheric circulation in the Banda Sea region: (1) the pre-northwest monsoon between October and November, (2) the northwest monsoon from December to March, (3) the monsoon transition in April, and (4) the southeast monsoon from May to September.

The pre-northwest monsoon period from October to November. This period is characterized by an increase in MLT, a shoaling of MLD, ILD, and BLT, saltier MLS, weaker wind (Fig. 1e), and reduced cloud coverage (Fig. 1f and g). The MLT increases from about 27°C in October to a maximum of above 30°C in November and December. The MLS is relatively unchanged at about 34 psu. MLD variability (black line in Fig. 1c and d) exhibits a similar pattern to that of MLT (blue line in Fig. 1c). MLD and MLT are negatively correlated, i.e. an increase in MLT is associated with a shallowing of the

MLD. A shallower MLD is observed during a period of weak wind speed. The MLD is < 30 m in October and reaches its minimum in November due to a minimum in wind stress (Fig. 1e). The outgoing longwave radiation (OLR) anomaly is positive, except in mid-late November, indicating reduced convective activity (Fig. 1f) and precipitation (Fig. 1g) throughout this period.

The northwest monsoon season from December to March. During this period, the Argo float data revealed that the MLT decreased by about 1 °C from December to March, albeit remaining above 29 °C. The high MLT is associated with energetic wind stress induced Ekman pumping that corresponds to negative vertical velocities indicative of downwelling-favorable conditions (Fig. 1e) and coincides with the thickening of the MLD and gradual deepening of the ILD. The difference between the MLD and ILD results in an increase of the BLT (~50 m). Short-term variations of the MLD from about 30 m to 70 m were also seen from January to March. These correspond with a slight decline in MLT, which appears to respond to more energetic winds aloft during the northwest monsoon period (Fig. 1e). The strong winds might increase surface buoyancy loss to the atmosphere (increased latent heat loss), contributing to this short-time MLD increase and MLT decrease. Simultaneously, the OLR anomaly is negative indicative of enhanced atmospheric convection and a significant rise in precipitation. The MLS is slightly declining though remained above 33.5 psu, except in March 2019 when a rapid fall of the MLS occurred. Nearly uniform salinity values below 34 psu are observed in the upper 100 m between March and April.

The monsoon transition period during April. With the exemption of ILD, BLT, and MLS, characteristics of MLD and MLT are similar to those of the pre-northwest monsoon. The transition period is marked by a second maximum of the MLT. The MLD becomes shallower (~20 m), while the ILD shows a similar variation with the BLT. The ILD and BLT were observed to deepen up to 80 m and 50 m, respectively, coinciding with a shorter period of weak winds, positive OLR and reduced precipitation. Despite suppressed convection and reduced precipitation, the MLS was at its lowest and reached a minimum value in April. Moreover, a significant reduction of the MLS to below 33 psu is observed in April 2019. Further analysis of the circulation in the IMC using the ocean reanalysis reveals that this minimum in salinity in 2019 can be attributed to the advection of low salinity water from the Java Sea into the Banda Sea (Additional file 1: Figure S1). The finding suggests that during this period, the advection of low salinity water controls the salt stratified layer which in turn lead to the development of the BLT.

The southeast monsoon season from May to September. This period is distinguished by steady winds corresponding to upwelling favorable conditions (Fig. 1c–e). These upwelling favorable conditions caused an uplift of the cooler (< 25 °C) and saltier (> 34 psu) water into the near surface layer (25 m). Figure 1c and d also shows a rapid drop in the MLT up to 2 °C and an increase in the MLS of about 0.5 psu. The MLT cooling was more intense in 2019 than in 2018. The ILD and MLD show a similar pattern and vary between 30 to 70 m and 20 to 60 m during the southeast monsoon, respectively. The BLT is observed to vary between 10 and 50 m as a result of the difference between the MLD and ILD. Daily OLR anomaly observed during this period changed from negative to positive between May and June and remained negative for the remainder of the season (Fig. 1f). This short-term change from more to less convective activity coincides with reduced precipitation in the eastern Banda Sea (Fig. 1g).

Balance of the MLT

The MLT balance for the eastern Banda Sea is displayed in Fig. 2a, along with the estimated terms on the right-hand side of Eq. 1 and with the sum of these three terms in Fig. 2b. Figure 2a shows alternating periods of strong warming (~2 °C month⁻¹) and cooling MLT tendencies (~ -2 °C month⁻¹) on seasonal time scales. The warming tendencies occur during periods of positive NSHF, conditions that occur more frequently during the pre-northwest monsoon season period from about October to November. The negative NSHF during the early southeast monsoon season from May to July coincides with a rapid cooling. The seasonality of each term of the MLT balance is summarized in Additional file 1: Table S1. The analysis finds that the seasonal cycle of the MLT tendency is controlled by NSHF (Fig. 2a). The NSHF exhibits a cycle which mimics that of the MLT tendency. The second contribution to the MLT tendency is the HTA term. The HTA is characterized by a seasonal cycle with a brief period of warming between December and March. This reflects the northwest monsoon wind-induced Ekman flow causing warm water accumulation in the eastern Banda Sea, as documented by Sprintall and Liu (2005). The third contribution to the MLT tendency is the VTE term. The vertical processes tend to cool the MLT tendency for a shorter period from October to December.

The sum of terms on the right-hand side of Eq. 1, i.e. NSHF, HTA, and VTE replicates the overall pattern of the MLT tendency (Fig. 2b) with a correlation of 0.74 and root mean square difference of 0.02 ± 0.01 °C month⁻¹. However, this MLT balance also indicates that unresolved and residual processes play a prominent

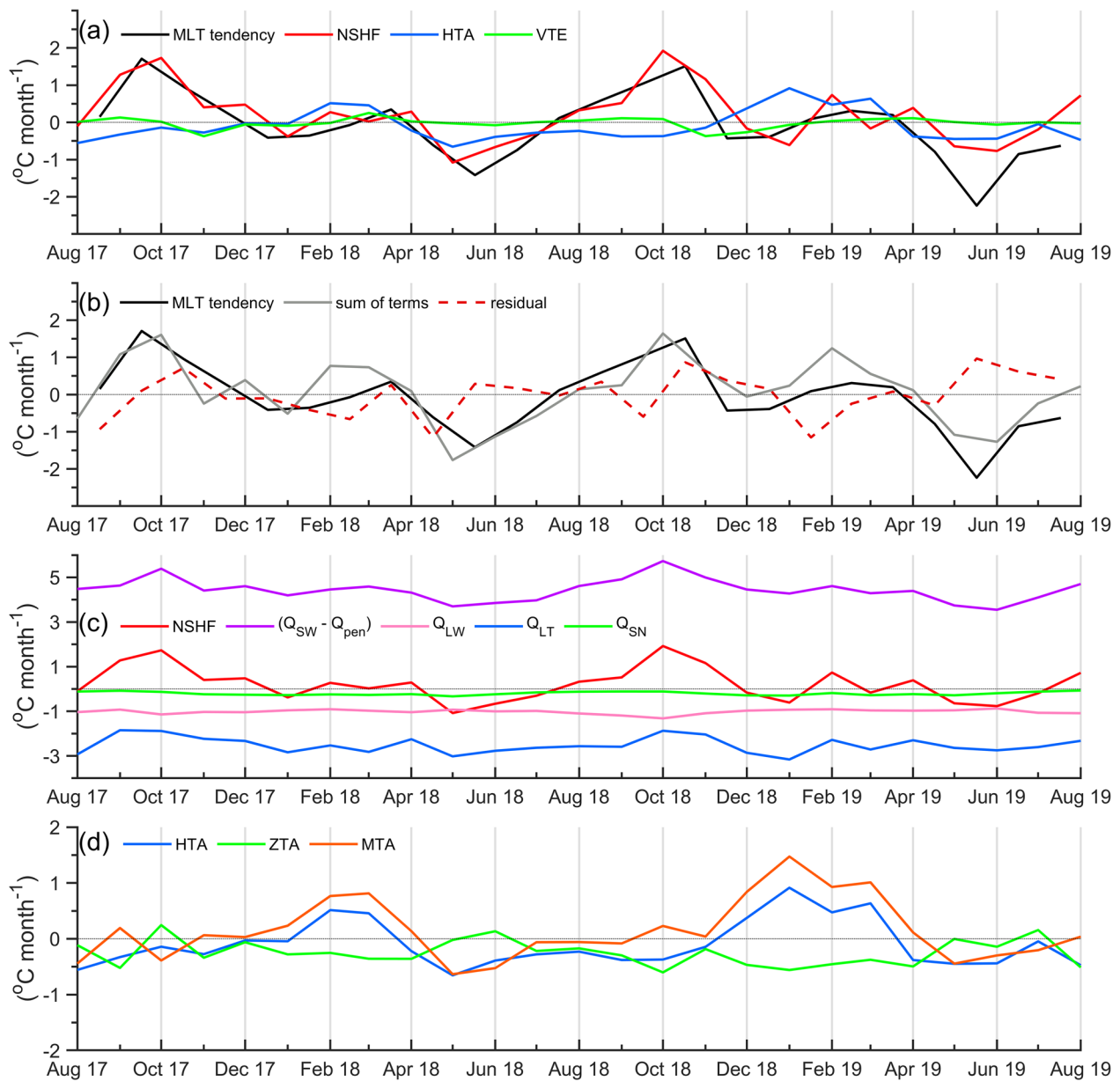


Fig. 2 **a** Temporal evolution of the MLT balance ($^{\circ}\text{C month}^{-1}$). MLT tendency (black line), net surface heat flux (NSHF (red line), horizontal temperature advection (HTA; blue line), and vertical temperature entrainment (VTE; green line). **b** MLT tendency (black line), sum of MLT balance terms (grey line), and residual (red dashed line). **c** Decomposition of NSHF into net shortwave radiation (Q_{SW}) minus the fraction of shortwave radiation that escapes through the base of the MLD (Q_{pen} ; purple line), net longwave radiation (Q_{LW} ; pink line), net latent heat flux (Q_{LT} ; blue line) and net sensible heat flux (Q_{SN} ; green line). **d** Decomposition of HTA into zonal temperature advection (ZTA; green line) and meridional temperature advection (MTA; orange line)

role in controlling MLT, particularly between January and June. In general, the most significant driver of MLT changes is the NSHF. This is in particular evident during the late southeast to pre-northwest monsoon from about September to November when the MLT tendency reaches a maximum of $\sim 1.75^{\circ}\text{C month}^{-1}$, and NSHF is the dominant contributor to the overall

warming of nearly $1.75^{\circ}\text{C month}^{-1}$. With the onset of the northwest monsoon season in December, HTA contributes $\sim 0.50^{\circ}\text{C month}^{-1}$ to the overall MLT tendency. The contribution from NSHF decreases which corresponds to a minimum in solar insolation. The MLT tendency is forced primarily by HTA. The late northwest and transition monsoon period from

March to April is characterized by a weak increase in NSHF that is only a quarter of the maximum amplitude during the late southeast and pre-northwest monsoon from September to November. During this time, HTA and NSHF contribute to warming the MLT tendency up to $\sim 0.50 \text{ }^\circ\text{C month}^{-1}$.

Throughout the southeast monsoon season from May to July 2018, all terms act to balance the MLT tendency (Fig. 2b). The Banda Sea loses heat to the atmosphere as indicated by a negative NSHF. NSHF decreases to its minimum of about $-0.60 \text{ }^\circ\text{C month}^{-1}$, concurrent with the slight cooling MLT tendency due to HTA and VTE at the base of the mixed layer contributing each about $-0.40 \text{ }^\circ\text{C month}^{-1}$. The combination of cooling from NSHF, HTA, and VTE results in a strong cooling tendency of the MLT exceeding $-1.50 \text{ }^\circ\text{C month}^{-1}$, particularly in June and July 2019 (Fig. 2b). These year-to-year differences are associated with interannual variability of NSHF and HTA. To gain further insight into the anomalous NSHF that drives the warming phase of the MLT tendency, it is decomposed into net shortwave radiation (Q_{SW}) minus the fraction of shortwave radiation that escapes through the base of the MLD (Q_{pen}), net longwave radiation (Q_{LW}), net latent heat flux (Q_{LT}), and net sensible (Q_{SN}) components.

The net surface heat flux shows a bimodal distribution that is essentially predominated by the shortwave heat flux from solar radiation and modulated by Q_{LT} (Fig. 2c). The first maxima of $Q_{\text{SW}} - Q_{\text{pen}}$ in October–November are considerably larger than the second maximum in March–April. This is due to the difference in the maximum insolation in the Banda Sea (Halkides et al. 2011). The decomposition of HTA into zonal temperature advection (ZTA) and meridional temperature advection (MTA) reveals that the MTA clearly prevails the ocean processes that contribute to the MLT tendency (Fig. 2d). Prominent warming tendencies ($\sim 0.75 \text{ }^\circ\text{C month}^{-1}$) due to MTA are observed during the northwest monsoon period from December to February but are opposed by steady negative ZTA ($\sim -0.25 \text{ }^\circ\text{C month}^{-1}$). This results in a low warming tendency of $\sim 0.50 \text{ }^\circ\text{C month}^{-1}$.

Balance of the MLS

Results from the MLS balance analysis suggest that the negative and positive MLS tendencies occur during the northwest and southeast monsoon, respectively (Fig. 3a). The MLS tendency reaches its minimum in February/March and maximum in May/June (Additional file 1: Table S2). The horizontal salinity advection (HSA) term emulates a similar pattern to that of the MLS tendency. It suggests that HSA is the main process controlling the MLS seasonal variability in the Banda Sea (Fig. 3a). From January to April, the HSA contributes to the negative

MLS tendency due to oceanic surface circulation that advects low salinity water from the Java Sea into the Banda Sea (Additional file 1: Fig. S1). Its effect on the MLS tendency reaches its maximum freshening values of about $-0.25 \text{ psu month}^{-1}$ and $-0.75 \text{ psu month}^{-1}$ from February to April 2018 and 2019, respectively. In contrast, HSA makes a positive contribution to the MLS tendency with the highest value of about $0.5 \text{ psu month}^{-1}$ between May and July. From December (August) to June (November) the negative (positive) net freshwater flux (FWF) reinforces (reduces) contribution made by HSA to the MLS tendency. The negative FWF indicates that the total oceanic freshwater gain is larger than freshwater loss due to evaporation. This results in a lower MLS in the Banda Sea. The vertical salinity entrainment (VSE) term in the MLS balance is much smaller than the FWF. Although this term is generally small, its influence becomes evident in April when it attains maximum freshening values.

As shown in Fig. 3b, the sum of FWF, HSA, and VSE is always greater than the MLS tendency, though it captures the seasonal evolution of the MLS tendency (black line). Substantial residuals are observed in all months. The correlation between the MLS tendency and the sum of all terms is 0.62 with a mean square difference of $0.01 \pm 0.01 \text{ psu month}^{-1}$. Dividing the HSA term into zonal salinity advection (ZSA) and meridional salinity advection (MSA), we find that the MSA dominates the ocean processes that contributed to the MLS tendency (Fig. 3c). The small positive contribution due to HSA ($< 0.25 \text{ psu month}^{-1}$) is due to the balance between positive MSA and negative ZSA, particularly during the pre-northwest and early northwest monsoon. Significant freshening tendencies ($< -0.25 \text{ psu month}^{-1}$) of the HSA are observed from February to April (Fig. 3c). During this time, MSA becomes negative while ZSA remains negative resulting in a maximum freshening effect of the HSA. From May to July each year, both MSA and ZSA make a positive contribution to the strongest positive HSA.

Summary and conclusions

In this study, we document the seasonal variability of the MLT, MLS, MLD, ILD, and BLT in the Banda Sea using data from a single Argo float (6901746) recorded between August 1, 2017 and August 28, 2019. The float provides the only available coherent long-term time series of in situ observations in the Banda Sea until now. The use of 25 months of Argo float data allows to investigate the upper ocean circulation and to estimate MLT and MLS balance for different monsoonal seasons. The MLT cooling was stronger in 2019 than in 2018, especially during the southeast monsoon from May to September. El Niño in 2019 likely contributes to this significant MLT

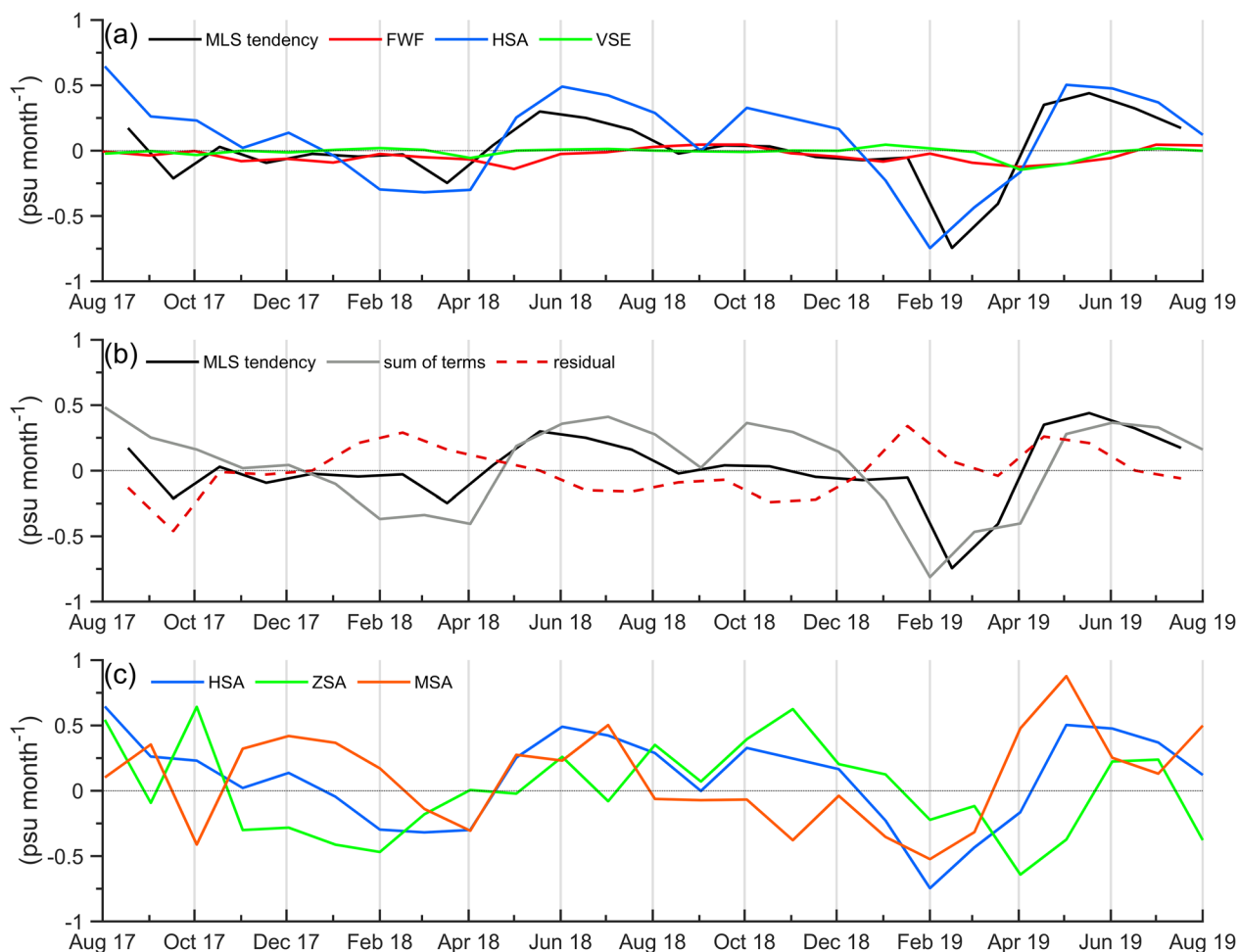


Fig. 3 Same as Fig. 2, but for the MLS balance (psu month⁻¹)

cooling. Gordon and Susanto (2001) reported that the coldest SST is driven by strong upwelling during El Niño. Further, Napitu et al. (2015) demonstrate the cooling phase of SST attributed to the active phase of MJO. The observed Argo trajectory reveals the presence of cyclonic and anticyclonic circulations. Zhu et al. (2019) suggest that these are forced by seasonally reversing monsoonal winds. The surface layer exhibits cyclonic (anticyclonic) circulation during the north-westerly (south-easterly) monsoon (Zhu et al. 2019). The monsoon wind also links to the seasonal variability of the Argo-derived ILD, MLD and BLT.

We quantify the physical processes that regulate the MLT and MLS variations in the Banda Sea using the heat and salt balance analysis from a single Argo similar to the work by Shee et al. (2019). To balance the MLT and MLS balance, a residual term exists. From the MLT balance analysis, we find that the contribution due to NSHF drives the maxima of the MLT warming tendency during the pre-northwest monsoon season between

October and November each year. Our analysis also finds that the MLT warming tendency is mainly due to heat gains via $Q_{SW} - Q_{pen}$. However, cooling due to HTA and residual is not negligible. From January to June, the residual components appear to be more important than HTA in the MLT balance. This residual likely corresponds with the turbulent mixing at the base of the mixed layer associated with horizontal and vertical eddy diffusion, as previously reported by Halkides et al. (2011). The results from this study provide credibility to slab ocean model findings by Halkides et al. (2011) and Napitu et al. (2015) that lacked any validation using in situ data.

The present analysis identifies a second maximum in the MLT warming tendency. It is a characteristic of the late northwest and transition monsoon season but disappears soon after the southeast monsoon season emerges in the Banda Sea. The MTA is mainly effective at enhancing the MLT warming tendency during this period. This advection is likely related to the Ekman transport inducing downwelling, leading to the

accumulation of warm water and MLD deepening in the Banda Sea (Sprintall and Liu 2005). The dominant MLT cooling tendency during the southeast monsoon season is explained by the combined effect of heat loss from the ocean (negative NSHF) and cooling due to HTA and VTE at the base of the mixed layer in association with the Ekman mass and heat flux (Sprintall and Liu 2005).

The seasonal MLS is largely dominated by HSA and residual rather than by the exchange of freshwater between the ocean and the atmosphere. This significant role of the residual components is likely associated with turbulent mixing due to horizontal and vertical eddy diffusion. For example, Halkides et al. (2011) demonstrated that wind-driven vertical eddy diffusivity/turbulent mixing increases from June to October (as illustrated by the MLD deepening in Fig. 1c), elevating the pycnocline and bringing relatively salty water from below into the mixed layer. Moreover, Halkides et al. (2011) also showed that HSA and VSE make comparable contributions to the seasonal MLS variations. This is probably due to differences in the MLS balance between the eastern and western parts of the Banda Sea. Note that this study is based on the Argo data in the eastern Banda Sea that does not fully capture the oceanic variability, including large HSA through the Flores Sea, in the western part of the Banda Sea as demonstrated early by Halkides et al. (2011).

Previous studies of the Banda Sea's MLT balance by Halkides et al. (2011) and Napitu et al. (2015) used slab ocean models and their analyses are limited due to a lack of in-situ observation data. Our analysis is the first study to quantify MLT and MLS balance and the associated processes in the Banda Sea using in situ data. Even though it is difficult to close MLT and MLS balance based on Argo float data in the eastern Banda Sea, the balance analysis reveals that the sum of atmospheric and oceanic flux terms generally compares well with the seasonal MLT and MLS tendency derived from observations. The sum of NSHF (FWF), HTA (HSA), and VTE (VSE) is strongly correlated with MLT (MLS) tendency in the study region. There is a difference between Argo-based MLT and MLS tendency and the estimated atmospheric and oceanic flux terms. The imbalance could result from unresolved residuals processes such as the heat flux at the bottom of the mixed layer due to radiative heat loss, horizontal and vertical eddy diffusion (Halkides et al. 2011; Oliver et al. 2021) as well as the possible errors in the other terms. However, within this limitation, the MLT and MLS balance provided a basis for understanding of the seasonal variability of MLT and MLS that could lead to improved forecasting weatherevents in the IMC. The results from this study provide a reference case for future

observational experiments and evaluations of ocean models for this region. This study also demonstrated the exceptional capability of a single Argo float in observing upper ocean processes in a region where long-term in situ observations are limited or non-existent.

Abbreviations

IMC	Indonesian maritime continent
ITF	Indonesian Throughflow
BLT	Barrier layer thickness
ILD	Isothermal layer depth
SST	Sea surface temperature
MJO	Madden-Julian oscillation
MLT	Mixed layer temperature
MLS	Mixed layer salinity
NSHF	Net surface heat flux
HTA	Horizontal temperature advection
ZTA	Zonal temperature advection
MTA	Meridional temperature advection
VTE	Vertical temperature entrainment
FWF	Freshwater flux
MLD	Mixed layer depth
OLR	Outgoing longwave radiation
QSW	Shortwave radiation
QLW	Longwave radiation
QLT	Latent heat flux
QSN	Sensible heat flux
HSA	Horizontal salinity advection
VSE	Vertical salinity entrainment
ZSA	Zonal salinity advection
MSA	Meridional salinity advection

Supplementary Information

The online version contains supplementary material available at <https://doi.org/10.1186/s40562-023-00266-x>.

Additional file 1. Figure S1. Monthly mean surface salinity (psu) and surface current from BRAN in the Indonesian Maritime Continent from February 2019 to July 2019. Black contour line represents the 500 m isobath. Blue dashed lines indicate the study domain. **Figure S2.** Time series of monthly (a) MLT (°C) and (b) MLS (psu) from the Argo float 6901746 (red lines), superimposed with collocated MLT and MLS from BRAN (blue lines). **Figure S3.** Daily SST (°C) from Argo float 6901746 (blue lines) and NOAA OI2 (red lines) in the Banda Sea from 1 August 2017 to 28 August 2019.

Acknowledgements

MFAI acknowledges support from GEOMAR Helmholtz Centre for Ocean Research Kiel and the National Research and Innovation Agency of Indonesia (BRIN). JK acknowledges funding by JPI-Climate and JPI Oceans project EUREC4A-OA. The authors would like to thank Agus Atmadipoera and Christine Coatanoan for their help regarding the Indonesian Argo program.

Author contributions

MFAI, TA, HC, and RA are the main contributor to this manuscript, who proposed the research topic, designed the study, and wrote the original draft. Other authors contributed to the data analysis, interpretations, reviewing and editing the manuscript. All authors read and approved the final manuscript.

Funding

This research is funded by the Georg Foster Research Fellowship of the Alexander von Humboldt-Stiftung. JK is supported by JPI-Climate and JPI Oceans project EUREC4A-OA.

Availability of data and materials

Argo data were collected and made freely available by the International Argo Program and the national programs that contribute to it (<http://www.argo.ucsd.edu>, <http://argo.jcommops.org>). The Argo Program is part of the Global Ocean Observing System of the Coriolis Data Assembly Center (<http://doi.org/10.17882/42182>). The Argo 6901746 data are available at <https://www.ocean-ops.org/board/wa/Platform?ref=6901746>. NOAA-OI2 SST data provided by the NOAA-ESRL Physical Sciences Laboratory from their website at <https://www.downloads.psl.noaa.gov/Datasets/noaa.oisst.v2.highres/>. Precipitation data are available at <https://doi.org/10.5067/GPM/IMERG/3B-HH/06>. Outgoing Longwave Radiation provided by the NOAA National Climatic Data Center. <https://doi.org/10.7289/V5SJ1HH2>. The wind products from the Copernicus Marine Environment Monitoring Service information can be found at <https://doi.org/10.48670/moi-00185>. ERA5 data for this research are available at the Copernicus Climate Change Service (C3S) Climate Data Store: <https://doi.org/10.24381/cds.adbb2d47>. The BRAN datasets are publicly available at <https://doi.org/10.25914/6009627c7af03>.

Declarations

Competing interests

The authors declare that they have no competing interests.

Received: 19 September 2022 Accepted: 13 February 2023

Published online: 23 February 2023

References

- Gordon AL, Susanto RD (2001) Banda Sea surface-layer divergence. *Ocean Dyn* 52:2–10. <https://doi.org/10.1007/s10236-001-8172-6>
- Halkides D, Lee T, Kida S (2011) Mechanisms controlling the seasonal mixed-layer temperature and salinity of the Indonesian seas. *Ocean Dyn* 61:481–495. <https://doi.org/10.1007/s10236-010-0374-3>
- Jochum M, Potemra J (2008) Sensitivity of tropical rainfall to Banda Sea diffusivity in the Community Climate System Model. *J Clim* 21:6445–6454. <https://doi.org/10.1175/2008JCLI2230.1>
- Kawamura R, Fukuta Y, Ueda H et al (2002) A mechanism of the onset of the Australian summer monsoon. *J Geophys Res Atmos* 107:ACL-5. <https://doi.org/10.1029/2001JD001070>
- Kida S, Richards KJ (2009) Seasonal sea surface temperature variability in the Indonesian Seas. *J Geophys Res Ocean* 114:C06016. <https://doi.org/10.1029/2008JC005150>
- Kim J, Jeong S, Kug J, Williams M (2019) Role of local air-sea interaction in fire activity over Equatorial Asia. *Geophys Res Lett* 46:14789–14797. <https://doi.org/10.1029/2019GL085943>
- Lee T, Fournier S, Gordon AL, Sprintall J (2019) Maritime Continent water cycle regulates low-latitude chokepoint of global ocean circulation. *Nat Commun* 10:1–13. <https://doi.org/10.1038/s41467-019-10109-z>
- Moisan JR, Niiler PP (1998) The seasonal heat budget of the North Pacific: net heat flux and heat storage rates (1950–1990). *J Phys Oceanogr* 28:401–421. [https://doi.org/10.1175/1520-0485\(1998\)028%3c0401:TSHBOT%3e2.0.CO;2](https://doi.org/10.1175/1520-0485(1998)028%3c0401:TSHBOT%3e2.0.CO;2)
- Napitu AM, Gordon AL, Pujiana K (2015) Intraseasonal sea surface temperature variability across the Indonesian Seas. *J Clim* 28:8710–8727. <https://doi.org/10.1175/JCLI-D-14-00758.1>
- Oliver ECJ, Benthuyzen JA, Darmaraki S et al (2021) Marine heatwaves. *Ann Rev Mar Sci* 13:1–30. <https://doi.org/10.1146/annurev-marine-032720-095144>
- Pei S, Shinoda T, Steffen J, Seo H (2021) Substantial sea surface temperature cooling in the Banda sea associated with the Madden-Julian oscillation in the boreal winter of 2015. *J Geophys Res Ocean* 126:1–19. <https://doi.org/10.1029/2021JC017226>
- Qu T, Du Y, Strachan J et al (2005) Sea Surface temperature and its variability in the Indonesian Region. *Oceanography* 18:50. <https://doi.org/10.5670/oceanog.2005.05>
- Shee A, Sil S, Gangopadhyay A et al (2019) Seasonal evolution of oceanic upper layer processes in the northern bay of Bengal following a single Argo float. *Geophys Res Lett* 46:5369–5377. <https://doi.org/10.1029/2019GL082078>
- Sprintall J, Liu WT (2005) Ekman mass and heat transport in the Indonesian seas. *Oceanography* 18:88. <https://doi.org/10.5670/oceanog.2005.09>
- Sprintall J, Tomczak M (1992) Evidence of the Barrier Layer in the Surface Layer of the Tropics ocean surface mixed layer generally denotes a quasi-kinetic energy and potential energy processes mentioned its degree state. *J Geophys* 97(C5):7305–7316. <https://doi.org/10.1029/92JC00407>
- Vijith V, Vinayachandran PN, Webber BGM et al (2020) Closing the sea surface mixed layer temperature budget from in situ observations alone: operation advection during BoBBLE. *Sci Rep* 10:1–12. <https://doi.org/10.1038/s41598-020-63320-0>
- Yoneyama K, Zhang C (2020) Years of the maritime continent. *Geophys Res Lett* 47:e2020GL087182. <https://doi.org/10.1029/2020GL087182>
- Yuan D, Li X, Wang Z et al (2018) Observed transport variations in the Maluku Channel of the Indonesian seas associated with western boundary current changes. *J Phys Oceanogr* 48:1803–1813. <https://doi.org/10.1175/JPO-D-17-0120.1>
- Yuan D, Yin X, Li X et al (2022) A Maluku Sea intermediate western boundary current connecting Pacific Ocean circulation to the Indonesian Throughflow. *Nat Commun* 13:1–8. <https://doi.org/10.1038/s41467-022-29617-6>
- Zhu Y, Wang L, Wang Y et al (2019) Stratified circulation in the Banda sea and its causal mechanism. *J Geophys Res Ocean* 124:7030–7045. <https://doi.org/10.1029/2019JC015279>

Publisher's Note

Springer Nature remains neutral with regard to jurisdictional claims in published maps and institutional affiliations.

Submit your manuscript to a SpringerOpen[®] journal and benefit from:

- Convenient online submission
- Rigorous peer review
- Open access: articles freely available online
- High visibility within the field
- Retaining the copyright to your article

Submit your next manuscript at ► [springeropen.com](https://www.springeropen.com)